Journal of Iron and Steel Research, International 24 (2017) 1223—1230

Contents lists available at ScienceDirect
Journal of Iron and Steel Research, International
journal homepage: www.chinamet.cn

Influence of bias voltage on structure, mechanical and corrosion properties of reactively sputtered nanocrystalline TiN films

Chun-lin He[1,*], Jin-lin Zhang[1], Guo-feng Ma[1], Zhao-fu Du[2], Jian-ming Wang[1], Dong-liang Zhao[2]
[1] Liaoning Provincial Key Laboratory of Advanced Materials, Shenyang University, Shenyang 110044, Liaoning, China
[2] Research Institute of Functional Materials, Central Iron & Steel Research Institute, Beijing 100081, China

ARTICLE INFO

Key words:
TiN film
Nanocrystalline
Bias voltage
Microstructure
Mechanical property
Corrosion resistance

ABSTRACT

Nanocrystalline TiN films were prepared by DC reactive magnetron sputtering. The influence of substrate biases on structure, mechanical and corrosion properties of the deposited films was studied using X-ray diffraction, field emission scanning electron microscopy, nanoindentation and electrochemical techniques. The deposited films have a columnar structure, and their preferential orientation strongly depends on bias voltage. The preferential orientations change from (200) plane at low bias to (111) plane at moderate bias and then to (220) plane at relatively high bias. Nanohardness H, elastic modulus E, H/E^* and H^3/E^{*2} ratios, and corrosion resistance of the deposited films increase first and then decrease with the increase in bias voltage. All the best values appear at bias of -120 V, attributing to the film with a fine, compact and less defective structure. This demonstrates that there is a close relation among microstructure, mechanical and corrosion properties of the TiN films, and the film with the best mechanical property can also provide the most effective corrosion protection.

1. Introduction

TiN films are widely used as protection coatings of cutting tools, molds and dies against abrasion, corrosion and oxidation[1,2]. They are generally produced by physical vapor deposition (PVD), and the relationship between depositing processes, microstructure and properties is investigated[3-6]. The mechanical properties and corrosion resistance of the sputtered films are strongly dependent on their microstructure affected by processing parameters[7-10]. In general, TiN films are inert and stable in most aggressive media. However, PVD films most often present growth related defects such as pinholes and pores, through which the substrate materials are attacked in corrosion media[11-13]. Therefore, for industrial applications, PVD films with a fine, homogeneous and compact structure are always desirable, especially for promoting corrosion resistance.

Although there has been much information about microstructure, mechanical and corrosion properties for PVD metal nitride films[14-16], it is not always consistent due to various processing parameters used. The films which have the best mechanical properties are mostly not with the best corrosion resistance[14,16] because their corrosion resistance is very sensitive to the pores or pinholes[13,17]. Moreover, previous researches have shown that the microstructure and properties of TiN-based multilayer films (e. g. TiN/Ti[14], TiN/AlN[18], TiN/CrN[19], TiN/ZrN[20], TiN/W_2N[21], TiN/TiAlN[22], etc.) are associated with the TiN single layer. Therefore, it is also important to prepare a monolithic TiN film with high quality in multilayer systems[6,21,23]. In this paper, nanocrystalline TiN thin films were prepared by DC reactive sputtering at various bias voltages, and the relationship among bias, structure, mechanical and corrosion performance of the resulting films was studied in detail. The results show that PVD film produced at a proper bias voltage can exhibit both high mechanical and corrosion performance due to its fine, dense and less defective structure, which is very useful for the application of nitride-based films in abrasive and corrosion protection fields.

2. Materials and Methods

2.1. Film preparation

Nanocrystalline TiN thin films were prepared on

* Corresponding author. Prof., Ph.D.
E-mail address: *cclhhe@126.com* (*C.L. He*).

Received 18 November 2016; Received in revised form 9 January 2017; Accepted 23 January 2017
Available online 15 December 2017
1006-706X/Copyright©2017, The editorial office of Journal of Iron and Steel Research, International. Published by Elsevier Limited. All rights reserved.

both Si (100) and 304 stainless steel substrates using DC reactive magnetron sputtering. The apparatus schematic diagram is presented in Fig. 1. The distance of the Ti (99.99%) target to the substrate was about 8 cm. The substrate was successively cleaned for 20 min in acetone, 10 min in ethanol and 5 min in deionized water by ultrasonic wave. The base and working pressures of the deposition chamber were 6.0×10^{-4} Pa and 0.5 Pa, respectively. Ar (99.999%) and N_2 (99.999%) gases were used with fixed flow rates of 30 mL/min and 4 mL/min, respectively. Ti thin interlayer was first deposited on the substrate in Ar gas atmosphere for 10 min to promote adhesion, and then the TiN layer was deposited atop in a mixture atmosphere of Ar and N_2 gases for 2 h. The bias voltage applied on the substrate changed between -50 and -155 V. During deposition, the substrate was kept at 300 ℃.

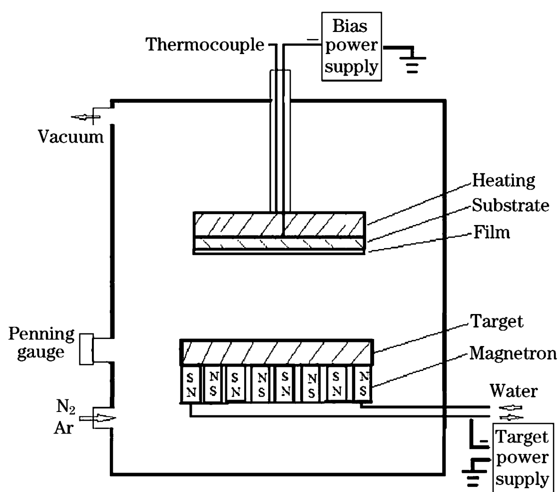

Fig. 1. Schematic diagram of experimental apparatus.

2.2. Film characterization

The film microstructure was examined by field emission scanning electron microscopy (FESEM S4800). The phase composition was characterized by X-ray diffraction (XRD, PANalytical B. V. X Pert Pro MPD) with CuKα radiation (wavelength of 0.15406 nm) operated at 40 kV and 40 mA. The grazing incident angle was 2°, the scanning angular (2θ) scope was 30°-90° and the scanning rate was 2(°)/min. Nanohardness and elastic modulus were measured by MTS XP nanoindenter system equipped with a Berkovich diamond indenter under 2 mN peak load, and mean values were obtained based on 5 indentations. The ratio of indentation depth/film thickness was no more than 0.1 in order to avoid the substrate effect.

Corrosion resistance was evaluated at 25 ℃ in 3.5% NaCl aqueous solution using PARSTAT 2273 advanced electrochemical system. The reference and auxiliary electrodes were a saturated calomel electrode and a graphite bar, respectively. Before measurements, the TiN specimens were put into the electrolyte solution until a steady open circuit potential (OCP) was recorded. Polarization curves were measured with a potential scanning rate of 0.332 mV/s, and electrochemical impedance spectroscopy (EIS) was recorded at OCP in frequency range between 10^5 Hz and 1 mHz by stimulating the specimens with an AC signal of 10 mV. The specimens were covered with electrical insulating paraffin except the surface for electrochemical measurements.

3. Results and Discussion

3.1. Microstructure

Fig. 2 presents the surface morphologies of the TiN films produced under different negative biases. It can be seen that the surface microstructures strongly depend on the biases, and both the surface roughness and compactness are improved when the negative bias increases from -50 to -120 V. However, too high negative bias (-155 V) may degrade the compactness and roughness as shown in Fig. 2(d) where some voids appear, arising from the ion bombardment effect on the surface mobility of adatoms. Some crystallites grow in the form of trigonal pyramids as well as relatively flat particles on the -50 V biased film surface (Fig. 2(a)), leading to a very rough surface with pinholes. This is in agreement with Ref. [5]. Obviously decreased microstructural defects and improved roughness with increasing negative bias voltages will improve film properties, especially corrosion resistance[13].

Fig. 3 shows the cross-section structures of the TiN thin films produced at different biases. The TiN thin films have a columnar structure. The average diameter of the columns decreases and the compactness is improved when the bias voltage increases. The column diameter appears to be finer at the film/substrate interface and enlarges slowly with increasing the distance from the interface. Similarly, the compactness is higher near the interface (Fig. 3).

Fig. 3 also shows the film thickness changes with bias voltage, which is closely related to the sputtering process[3]. Under lower bias voltage, the ion current density increases with increase in bias voltage; therefore, the film thickness increases from 0.77 μm at -50 V to its maximum value of about 1.01 μm at -85 V. Further increasing bias voltage can enhance re-sputtering effect which can hinder the film growth[7,8], causing almost no change in the film thickness with bias voltage between -85 V and -120 V. When the bias voltage further increases, the re-sputtering effect becomes remarkable and finally leads to obviously decreased film thickness (0.88 μm at -155 V).

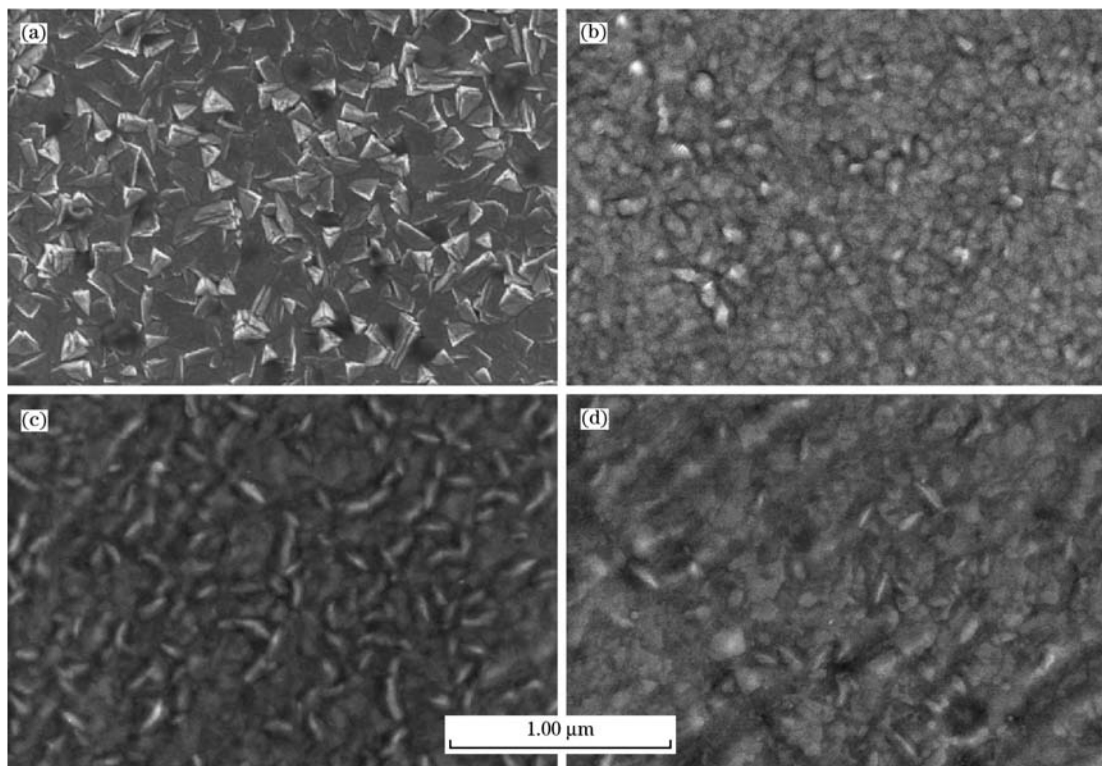

(a) －50 V; (b) －85 V; (c) －120 V; (d) －155 V.

Fig. 2. FESEM surface morphologies of TiN films produced at varying biases on Si (100) substrate.

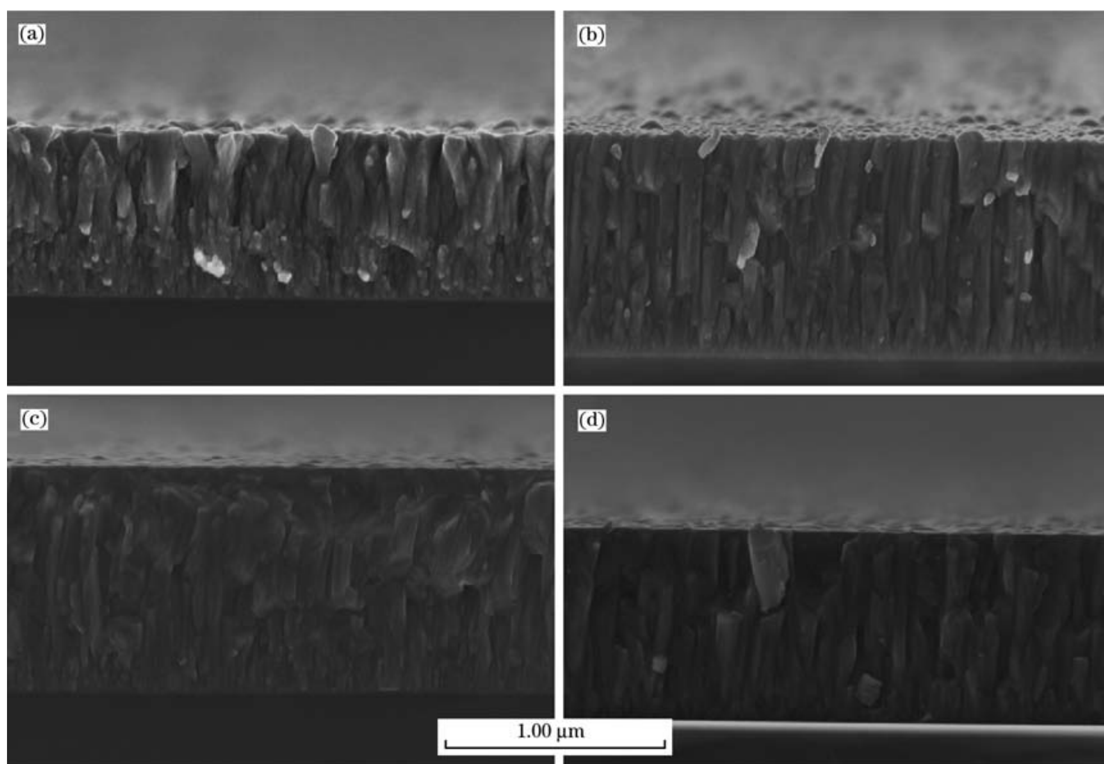

(a) －50 V; (b) －85 V; (c) －120 V; (d) －155 V.

Fig. 3. FESEM cross-section morphologies of different biased TiN films on Si (100) substrate.

Fig. 4 presents the XRD patterns of the different biased films. The peaks around 43.6°, 44.3°, and 50.7° correspond to the stainless steel substrate, and the other peaks can be ascribed to (111), (200), (220), (311)

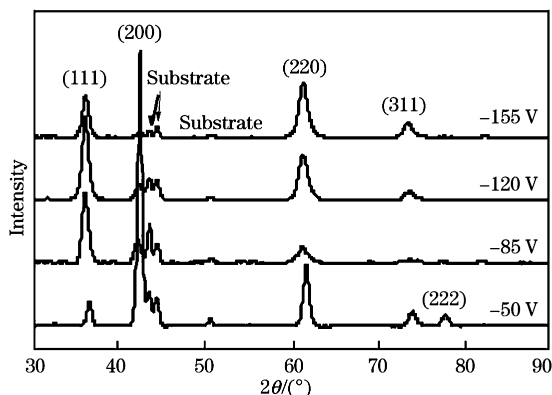

Fig. 4. XRD patterns of TiN films *vs*. negative bias voltages.

and (222) planes of B1-NaCl TiN structure. No peaks of Ti and Ti_2N are found. All these diffraction peaks are relatively broad, and the preferential orientations depend on the negative bias voltages.

For better comparing the influence of negative biases on crystal preferential orientation, texture coefficient T is introduced[24]:

$$T(hkl)=\frac{I(hkl)/I^0(hkl)}{(1/n)\sum I(hkl)/I^0(hkl)} \tag{1}$$

where, $I(hkl)$ and $I^0(hkl)$ stand for the diffraction intensity of the TiN film and theoretical intensity of the (hkl) plane, respectively; and n is the diffraction peak number. Table 1 presents the texture coefficients as a function of bias voltages obtained based on Eq. (1). In theory, the (200) planes of transition metal nitride with B1-typed NaCl structure have the lowest surface energy[25], leading to an obvious preferential orientation in this plane. Increasing negative bias voltage corresponds to a high energy of moving species, which can cause a strong orientation in the (111) plane, as the films biased at −85 and −120 V. As the negative bias increases to −155 V, the preferential orientation is changed into (220) plane. The change of preferential orientation can be attributed to two aspects as follows.

Firstly, during the PVD film growth, the texture evolution is associated with the competition between the surface and deformation energies. If the former dominates in the whole energy, the film grows along the (200) orientation. When the latter dominates, the (111) orientation is predominant[26]. Whereas, for the −155 V biased film with (220) preferential orientation, it is believed that the energy E_{bi} from bombarding ions exceeds the threshold value required to produce a film with a preferential orientation of (220) plane. Maybe this is due to a similar effect with an increase of energy E_{bi} arising from increasing N_2 partial pressure as observed by Musil[27].

Secondly, the ions, whose energy is proportional to bias voltage, will sputter the growing film when they impinge on it. Because their energies are relatively low, the ions may preferentially sputter the outer atoms of the film. In this case, the grains with the densest plane parallel to the film surface may be preferentially sputtered. Since the (111) plane is the densest plane (3.32 atoms/a^2), the grains on it will be preferentially sputtered. On the contrary, the grains will be sputtered at a reduced rate if the plane, parallel to the film surface, is less dense (e. g. (220): 2.12 atoms/a^2, or (200): 2.0 atoms/a^2) and permit the ions to enter into the crystal lattice. Consequently, the (111) texture sharply decreases while the (220) texture markedly increases as the bias voltage surpasses −85 V.

The negative bias voltages also strongly affect the grain size of TiN thin film. Fig. 5 shows the mean grain size of the TiN film computed according to the Scherrer's formula relative to the (111) plane. The gain sizes are in the range from 10 to 16 nm. The grain size drops quickly as the bias increases from −50 to −85 V, and it almost does not change with further promoting the bias. At higher biases, the grain refinement can be contributed to the penetration of impinging ions into the TiN lattice and the increased generation of defects for preferred nucleation places[8].

Table 1
Changes of preferential orientation coefficient with negative bias voltages

Bias/V	$T(111)$	$T(200)$	$T(220)$	$T(311)$
−50	0.30	2.00	1.02	0.67
−85	2.34	0.64	0.69	0.33
−120	1.72	0.24	1.32	0.72
−155	0.99	0.13	1.91	0.97

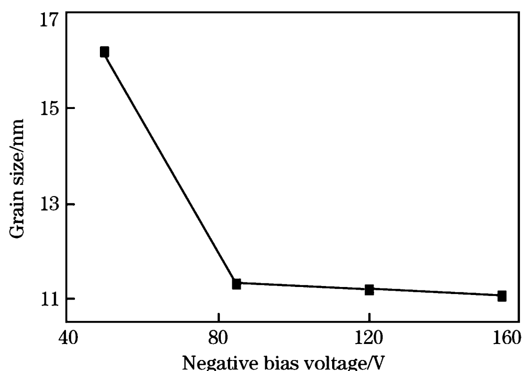

Fig. 5. Grain sizes for TiN films *vs*. bias voltages.

3.2. Mechanical properties

Fig. 6 presents the variations of nanohardness (H) and elastic modulus (E) of the TiN films with bias voltages. When the bias increases, H linearly increases first and then slightly decreases. Both the highest H value of (28.2±1.6) GPa and the highest

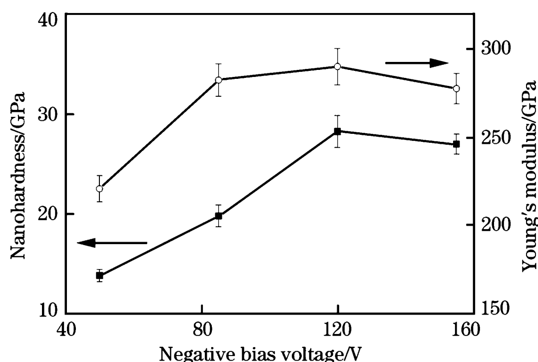

Fig. 6. Hardness and moduli of TiN films *vs.* negative bias voltages.

E value of (290.0±10.3) GPa occur at −120 V bias voltage, attributing to its finer and denser structure[28]. When the bias increases up to −155 V, the re-sputtering effect increases, resulting in increasing defects in the film and thus the nanohardness begins to decrease.

H/E^* and H^3/E^{*2} ratios can be used to characterize elastic strain to failure resistance and plastic deformation resistance of the film, which can be used to predict the abilities to resist mechanical degradation and failure of nanocrystalline films[19,29]. Here $E^*=E/(1-v^2)$ represents the film effective elastic modulus, and v represents the film Poisson's ratio. Fig. 7 indicates the variations of H/E^* and H^3/E^{*2} with negative bias voltages. The evolution trends for both H/E^* and H^3/E^{*2} with biases are similar to H. The −120 V biased film presents the greatest H/E^* and H^3/E^{*2}, indicating that such film possesses higher mechanical degradation and failure resistance. This can be attributed to the refinement of columnar structure and compressive stress[27,30]. Too high bias voltage, however, can introduce defects (Figs. 2(d) and 3(d)), resulting in decreasing the H/E^* and H^3/E^{*2} values to some extent.

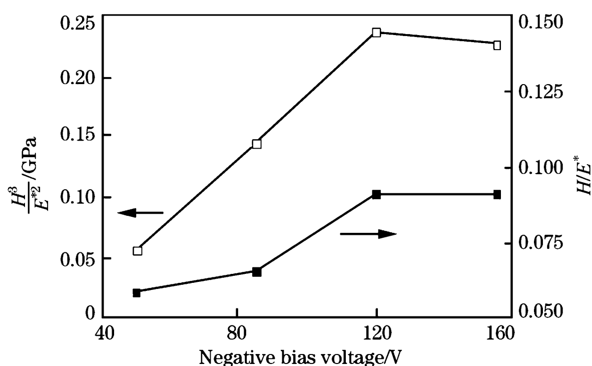

Fig. 7. H/E^* and H^3/E^{*2} values *vs.* bias voltages.

3.3. Corrosion resistance

Potentiodynamic polarization curves for the TiN thin films produced under different biases in 3.5% NaCl aqueous solution are shown in Fig. 8 and the related parameters are listed in Table 2. As seen from Table 2, the corrosion current density (I_{corr}) values are 0.038, 0.025, 0.0129 and 0.0355 μA · cm^{-2} for −50, −85, −120 and −155 V biased TiN films, respectively. Same trends are found for the corrosion potentials E_{corr}, the corrosion rate R_{corr} and polarization resistance R_p. These results indicate that the deposited films process an excellent corrosion resistance, which increases with increasing bias voltage up to −120 V, then decreases when the negative biases further increase. The best corrosion resistance is provided by the −120 V biased film, resulting from its fine, dense, and uniform microstructure[13,31]. Generally, film structural defects e. g. pinholes can provide a direct path for the corrosion media to reach the film/substrate interface, leading to the formation of corrosion microcell between the film and substrate[32]. Additionally, the poor corrosion resistance for reactive sputtered TiN films prepared at lower bias voltages may be associated with a non-uniform distribution of N^+ ions in the film surface, which leads to an increased defects in the film[33]. At moderate high bias voltages, fine, dense and stoichiometric composition films are formed, which can exhibit better corrosion resistance. Fig. 8 also clearly shows that all the TiN films exhibit a self-passivation behavior due to the formation of TiO_2[13,31,34] which probably results from the oxidation of TiN and Ti interlayer at structural defects[13].

Fig. 9 shows EIS plots of the TiN films exposed in

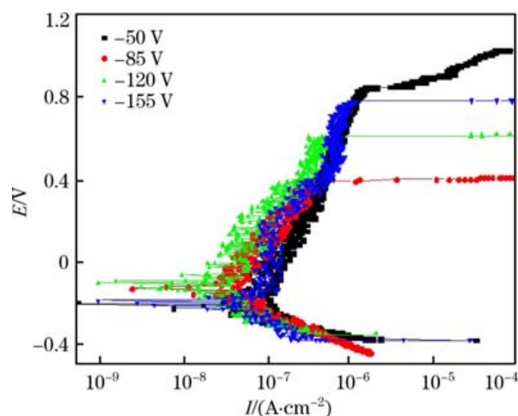

Fig. 8. Potentiodynamic polarization curves of TiN films *vs.* negative biases.

Table 2
Relative electrochemical parameters obtained from Fig. 8

Bias/ V	I_{corr}/ (μA · cm^{-2})	E_{corr}/ V	E_{pit}/ V	R_p/ (MΩ · cm^2)	R_{corr}/ (mm · a^{-1})
−50	3.80×10^{-2}	−0.228	0.843	0.9312	6.58×10^{-10}
−85	2.50×10^{-2}	−0.142	0.391	1.948	1.63×10^{-10}
−120	1.29×10^{-2}	−0.128	0.601	2.774	1.44×10^{-10}
−155	3.55×10^{-2}	−0.194	0.773	0.9474	5.05×10^{-10}

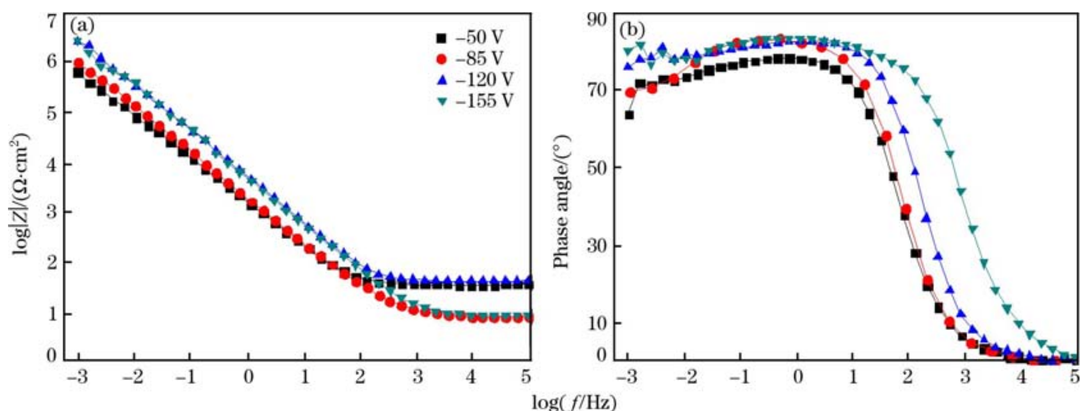

Fig. 9. EIS plots of TiN films change with negative bias voltages.

3.5% NaCl solution. The absolute values of the impedance increase with increasing bias voltages, resulting from the less defected films[9]. It can be seen that the spectra for the films show distinctive capacitance loops at a wide range of frequency, illustrating almost undamaged surface during the test period. The EIS for the TiN films is simulated well with an equivalent circuit shown in Fig. 10, where R_s represents the solution resistance; C_f and R_{pore} represent the capacitance and the pore resistance of the TiN films, respectively; C_{dl} and R_{ct} stand for the capacitance of double layer and charge transfer resistance of the substrate at the film/substrate interface at pores, respectively. Here, constant phase elements, Q_f and Q_{dl}, are used to replace C_f and C_{dl} in order to obtain a better dada fitting.

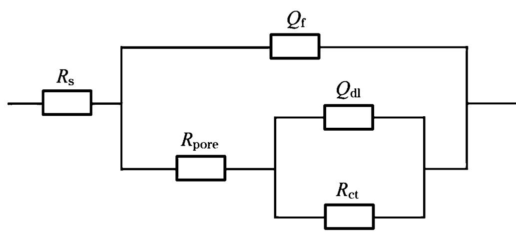

Fig. 10. Equivalent circuit for fitting EIS of TiN films.

Table 3 shows EIS simulation parameters for the TiN films and the uncoated substrate in NaCl solution. As seen from Table 3, the capacitance element of the films, Q_f-Y_0, is strongly dependent on the bias voltages, and sharply decreases with increasing bias up to －120 V and then slightly increases again, indicating that a homogeneous surface is gained at －120 V bias voltage in the present study. The capacitance C of a parallel-plate capacitor with a dielectric between its plates is $C=\varepsilon\varepsilon_0 A/d$, where ε is the dielectric constant, ε_0 is the permittivity of empty space, A is the plate area, and d is the distance between the parallel plates. For the TiN films, film thickness increases with increasing bias voltages up to －120 V and then slightly decreases, which should result in a corresponding decrease in capacitance. However, the change of d value is not great, so a sharp decrease in $Q_f-Y_0\approx C$ (Table 3) further reflects that A (surface area of film) decreases very quickly with increasing negative bias voltages within －120 V, indicating that much more homogeneous and less defective surfaces are being gained as the bias voltage increases. Unlike Q_f-Y_0, n_f value exhibits an inverse change with negative bias voltage, the biggest n_f present at －120 V represents a reduced dispersion. The highest value in R_{pore} for the film produced at －120 V bias voltage indicates that this film has the best corrosion resistance and fewest defects.

Table 3
EIS data simulations for TiN films

Bias/V	R_s/(Ω·cm²)	Q_f-Y_0/(F·cm⁻²)	n_f	R_{pore}/(Ω·cm²)	$Q_{dl}-Y_0$/(F·cm⁻²)	n_{dl}	R_{ct}/(Ω·cm²)
－50	22.07	1.903×10^{-4}	0.8875	2.124×10^{5}	6.606×10^{-5}	1	4.783×10^{5}
－85	11.23	6.978×10^{-5}	0.9055	3.897×10^{5}	1.772×10^{-5}	1	2.657×10^{6}
－120	25.95	5.532×10^{-5}	0.9315	4.808×10^{5}	1.172×10^{-5}	0.975	2.964×10^{6}
－155	6.633	5.702×10^{-5}	0.9204	4.521×10^{5}	1.314×10^{-5}	1	2.619×10^{6}

Table 3 also shows that the double layer capacitance, $Q_{dl}-Y_0$, gradually decreases and R_{ct} increases with increasing the bias voltages within －120 V, indicating a reduced corrosion rate[9]. This is because the area of through film pinholes decreases with the increase in bias voltages. Therefore, the EIS data in Table 3 clearly reflect the structural characteristics of the TiN thin films very well.

Fig. 11 presents the typical corrosion morphologies of the －120 V biased TiN film after polarization test. Actually, for all the different biased TiN films, the corrosion morphologies have similar features. The only difference is that the number of large pits is more for the higher biased films. There appear few but big pits on the corroded surface (Fig. 11(a)), related to big structural defects or weakness spots containing lots of through film pinholes in the film, through which the pits easily appear because galvanic corrosion takes place at the interface of the film/substrate[17]. Consequently, corrosion products can be formed and accumulated, and a local stress appears and continuously increases at the interface until a piece of TiN film peels off as seen in Fig. 11(b). During the tests, the film peeling is also visible to the naked eye. Similar peeling phenomena were observed on corroded PVD TiN[33,35], TiAlN[11], TiN/NbN[35] and TiAlN/CrN[11] films. At the places away from the peeling spots, the film is almost intact (Fig. 11(b)). The above results show that it is very useful for improvement in corrosion resistance to decrease large structural defects or through film pinholes in the sputtered TiN films.

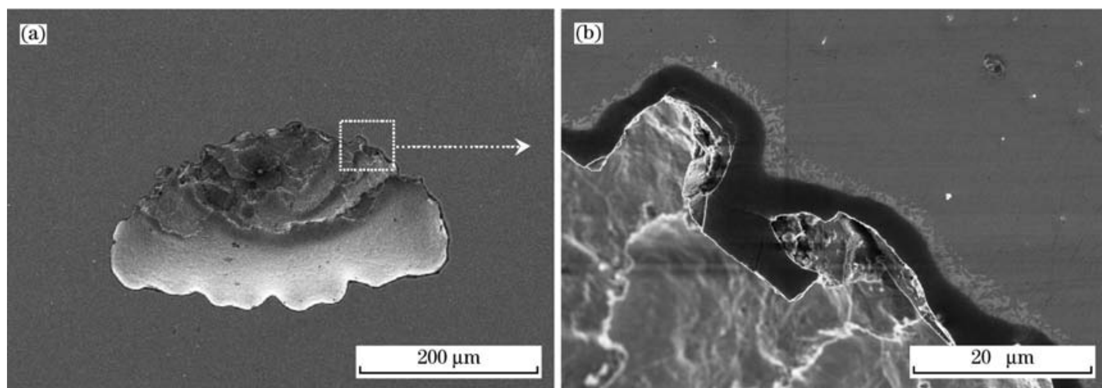

Fig. 11. Corrosion morphology of －120 V biased film after polarization test (a) and local magnification image showing film detachment (b).

4. Conclusions

(1) When negative bias voltages increase, the grain of the nanocrystalline TiN films becomes fine, the film thickens, and the compactness and roughness are improved. However, too high negative bias voltage can cause a strong resputtering, resulting in a rough surface, low compactness and reduced thickness. The finest and densest structure appears at －120 V biased film.

(2) The nanocrystalline TiN films have a columnar structure. The preferential orientation strongly depends on bias voltage and changes from (200) plane at low bias to (111) plane at moderate bias, and then to (220) plane at high bias voltage.

(3) The hardness, modulus, H/E^* and H^3/E^{*2} values of the nanocrystalline TiN thin films first increase and then decrease when the bias increases. The maximum values all appear at －120 V biased film.

(4) The corrosion resistance of the nanocrystalline TiN films first increases and then decreases with increase in the negative biases. The best protection efficiency is provided at the －120 V biased film resulting from its finer, denser and more homogenous structure. Few but large pits emerge on the corrosive surface, probably related to large structure defects or weakness spots containing lots of through film pores and pinholes.

Acknowledgment

This work was supported by the National Natural Science Foundation of China (51171118).

References

[1] A. Bahri, E. Kaçar, S. S. Akkaya, K. Elleuch, M. Ürgen, Surf. Coat. Technol. 304 (2016) 560-566.
[2] W. Xiang, C. Zhao, K. Liu, G. Zhang, K. Zhao, J. Alloy. Compd. 658 (2016) 862-866.
[3] N. Jiang, H. J. Zhang, S. N. Bao, Y. G. Shen, Z. F. Zhou, Physica B 352 (2004) 118-126.
[4] P. Chen, X. Xiang, T. M. Shao, Y. Q. La, J. L. Li, Appl. Surf. Sci. 389 (2016) 361-368.
[5] B. Pecz, N. Frangis, S. Logothetidis, I. Alexandrou, P. B. Barna, J. Stoemenos, Thin Solid Films 268 (1995) 57-63.
[6] H. Liang, J. Xu, D. Zhou, X. Sun, S. Chu, Y. Bai, Ceram. Int. 42 A (2016) 2642-2647.
[7] D. M. Devia, E. Restrepo-Parra, P. J. Arango, A. P. Tschiptschin, J. M. Velez, Appl. Surf. Sci. 257 (2011) 6181-6185.
[8] X. Chen, Y. Xi, J. Meng, X. Pang, H. Yang, J. Alloy. Compd. 665 (2016) 210-217.
[9] N. D. Nam, J. G. Kim, W. S. Hwang, Thin Solid Films 517 (2009) 4772-4776.
[10] C. Yu, L. Tian, Y. Wei, S. Wang, T. Li, B. Xu, Appl. Surf. Sci. 255 (2009) 4033-4038.
[11] V. K. William Grips, H. C. Barshilia, V. Ezhil Selvi, Kalavati, K. S. Rajam, Thin Solid Films 514 (2006) 204-211.
[12] D. Zhang, L. Duan, L. Guo, W. H. Tuan, Int. J. Hydrogen Energy 35 (2010) 3721-3726.
[13] C. Liu, Q. Bi, A. Matthews, Corros. Sci. 43 (2001) 1953-1961.
[14] M. Flores, S. Muhl, L. Huerta, E. Andrade, Surf. Coat. Technol. 200 (2005) 1315-1319.

[15] C. H. Hsu, C. Y. Lee, Z. H. Lin, W. Y. Ho, C. K. Lin, Thin Solid Films 519 (2011) 4928-4932.
[16] J. W. Lee, S. T. Chang, H. W. Chen, C. H. Chien, J. G. Duh, C. J. Wang, Surf. Coat. Technol. 205 (2010) 1331-1338.
[17] C. L. He, J. L. Zhang, J. M. Wang, G. F. Ma, D. L. Zhao, Q. K. Cai, Appl. Surf. Sci. 276 (2013) 667-671.
[18] D. Q. Yin, Y. Yang, X. H. Peng, Y. Qin, Z. C. Wang, Physica E 63 (2014) 125-130.
[19] Y. X. Ou, J. Lin, H. L. Che, W. D. Sproul, J. J. Moore, M. K. Lei, Surf. Coat. Technol. 276 (2015) 152-159.
[20] M. Naddaf, B. Abdallah, M. Ahmad, M. A-Kharroub, Nucl. Instr. Meth. Phys. Res. B 381 (2016) 90-95.
[21] C. L. Chang, T. H. Chiou, P. H. Chen, W. C. Chen, C. T. Ho, W. Y. Wu, Surf. Coat. Technol. 303A (2016) 25-31.
[22] E. Alat, A. T. Motta, R. J. Comstock, J. M. Partezana, D. E. Wolfe, J. Nucl. Mater. 478 (2016) 236-244.
[23] J. J. Yang, F. F. Zhang, Q. Wan, C. Y. Lu, M. J. Peng, J. L. Liao, Y. Y. Yang, L. M. Wang, N. Liu, Appl. Surf. Sci. 389 (2016) 255-259.
[24] D. N. Lee, J. Mater. Sci. 24 (1989) 4375-4378.
[25] P. Patsalas, C. Charitidis, S. Logothetidis, Surf. Coat. Technol. 125 (2000) 335-340.
[26] S. Q. Rong, J. He, H. J. Wang, C. X. Tian, L. P. Guo, D. J. Fu, Plasma Sci. Technol. 11 (2009) 38-41.
[27] J. Musil, in: Albano Cavaleiro, Jeff Th. M. De Hosson (Eds.), Nanostructured Coatings, Springer Science & Business Media, New York, 2006, pp. 407-463.
[28] A. M. Pagon, J. G. Partridge, P. Hubbard, M. B. Taylor, D. G. McCulloch, E. D. Doyle, K. Latham, J. E. Bradby, K. B. Borisenko, G. Li, Surf. Coat. Technol. 204 (2010) 3552-3558.
[29] J. Musil, F. Kunc, H. Zeman, H. Polakova, Surf. Coat. Technol. 154 (2002) 304-313.
[30] S. Zhang, D. Sun, Y. Q. Fu, H. J. Du, Surf. Coat. Technol. 198 (2005) 2-8.
[31] L. Cunha, M. Andritschky, L. Rebouta, R. Silva, Thin Solid Films 317 (1998) 351-355.
[32] S. H. Ahn, J. H. Lee, J. G. Kim, J. G. Han, Surf. Coat. Technol. 177-178 (2004) 638-644.
[33] C. V. Franco, L. C. Fontana, D. Bechl, A. E. Martinelli, J. L. R. Muzart, Corros. Sci. 40 (1998) 103-112.
[34] S. Rudenja, J. Pan, I. O. Wallinder, C. Leygraf, P. Kulu, J. Electrochem. Soc. 146 (1999) 4082-4086.
[35] H. C. Barshilia, M. S. Prakash, A. Poojari, K. S. Rajam, Thin Solid Films 460 (2004) 133-142.